Solid-State Interphases Design for High-Safety, High-Voltage and Long-Cyclability Practical Batteries via Ethylene Carbonate-Free Electrolytes

Yu Wu,[1,2,*] Wenjie Zhang,[1,2] Yalun Li,[3] Xuning Feng,[3,*] Zhuang Ma,[1,2] Dongsheng Ren,[3] Languang Lu,[3] Gui-Liang Xu,[4] Khalil Amine,[4] and Minggao Ouyang[3,*]

[1] School of Materials Science and Engineering, Beijing Institute of Technology, Beijing 100081, China.
[2] National Key Laboratory of Science and Technology on Materials under Shock and Impact, Beijing Institute of Technology, Beijing 100081, China.
[3] State Key Laboratory of Intelligent Green Vehicle and Mobility, Tsinghua University, Beijing 100084, China.
[4] Chemical Sciences and Engineering Division, Argonne National Laboratory, Lemont, IL 60439, USA.
Corresponding authors: wy15201240029@163.com; fxn17@mail.tsinghua.edu.cn; ouymg@mail.tsinghua.edu.cn

ABSTRACT
Ethylene carbonate (EC) plays a crucial role in current electrolytes for batteries. However, EC reacts exothermically with the electrode to trigger thermal runaway and undergoes continuous oxidative decomposition at high voltages, hindering it application for next-generation batteries. Here we report a simple and effective strategy to design sulfolane(SL)-based electrolyte with reshaped anions-dominated solvation structure, forming highly stable inorganic-dominated electrode-electrolyte interphases that efficiently stabilize nickel-rich cathode and graphite anode. Compared with the conventional electrolyte, practical pouch-type $LiNi_{0.8}Co_{0.1}Mn_{0.1}O_2$|Graphite cell with SL-based electrolyte significantly improve self-generated heat T_1 and thermal runaway triggering T_2 by 9.6 and 42.0 °C, respectively. More surprisingly, the pouch cell with SL-based electrolyte exhibits outstanding capacity retention of 88% after 1000 cycles charged up to 4.5 V. The study brings new insights for unlocking advanced electrolyte candidates to build next-generation practical safer high-energy batteries.

Keywords：
SL-based electrolyte; Solvation structure; High-safety; High-voltage; Long-cyclability

INTRODUCTION

To facing the ever-increasing requirement for electric vehicles and smart electric grids, tremendous efforts have been devoted to constructing safer high energy density Li-ion batteries (LIBs).[1-5] Electrolyte, as the "blood" of LIBs, plays an indispensable and important role in safe and efficient operation .[6,7] The state-of-the-art electrolyte in LIBs contains the indispensable ethylene carbonate (EC) solvent component to stabilize graphite anodes.[8] However, EC solvent undergo continuous oxidation reaction at high voltages because of the synergistic effect of thermodynamic limitations and catalytic nickel-rich layered oxide cathode surface, which severely restrict the energy density.[9-

[12] Beyond that, EC solvent can violently react with oxygen originated from aggressive nickel-rich cathodes to generate enormous heat, resulting in serious safety concerns related by thermal runaway (TR).[13-16] The current EC-based electrolyte system has been in use for 30 years,[17] but it is far from meeting the safer high energy density requirements of next-generation LIBs. The most urgent task is to design advanced EC-free electrolyte by removing the EC from the state-of-the-art EC-based electrolyte for next-generation LIBs.

Among numerous candidates, the sulfolane (SL) is expected to be an ideal electrolyte solvent for high voltage and high safety LIBs owing to intrinsic high dielectric constant, high oxidation stability, and non-flammability.[18-20] Unfortunately, its practical applications are restricted by the high viscosity and failure to passivate graphite anodes.[21,22] Recently, enormous achievements have been made in concentrated electrolyte system by enhancing the salt concentration, which not only signally regulates the Li^+ solvation structure dominated by anions but also dramatically switches the interphase chemistry on the electrode.[23-25] It is believed that due to the unique anions-dominated solvation structure of concentrated electrolyte, the formed inorganic-rich electrode-electrolyte interphase (EEI) derived from salt anion can effectively stabilize the electrode. However, the shortcoming of high viscosity limits the further application.[26] Several improvements were made to address the problem by adding the nonsolvating diluent, which not only maintains the unique solvation structure dominated by anions, but also reduces the viscosity and improves the wettability.[26-29] Therefore, it is a very appealing approach to design high performance SL-based electrolyte by rejuvenating solvation structure. Unfortunately, high-voltage and long cyclability practical safer pouch-type LIBs with SL-based electrolytes have not been reported so far.

Herein, we design high-voltage, high-safety, and long cyclability practical $LiNi_{0.8}Co_{0.1}Mn_{0.1}O_2$|Graphite (NCM811|Gr) pouch cells by employing SL-based electrolyte (1.2M LiFSI in SL/HFE (4:6)) with reshaped anions-dominated solvation structure, which can efficiently stabilize NCM811 cathode and Gr anode. The designed pouch cell presents superior high-voltage and long-term cyclability, that is, 88% capacity retention after 1000 cycles at 4.5V. In sharply contrast, the pouch cell with conventional electrolyte undergoes only 400 cycles and then rapidly decays in a "diving" manner. Moreover, pouch cell employing SL-based electrolyte can signally enhance self-generated heat T_1 by 9.6 ^oC, enhance TR triggering T_2 by 42.0 ^oC, and decrease the TR highest T_3 by 55.6 ^oC. The above-mentioned outstanding properties attributed to the substitution of the SL solvent for the EC solvent and construction of stable anions-derived inorganic-rich EEI, significantly protect electrode from side reactions. The study sheds light on the SL-based electrolyte with reshaped Li^+ solvation structure for practical safer high-energy density LIBs.

RESULTS AND DISCUSSION

First, we prepared a series of SL single solvent electrolytes with different LiFSI salt concentrations, including 1M-LiFSI-SL (1.0 M LiFSI in SL) and 3M-LiFSI-SL (3.0 M LiFSI in SL). After adding a certain amount of HFE nonsolvating solvent to dilute the

3M-LiFSI-SL, 1.2M-LiFSI-SL/HFE (1.2M LiFSI in SL/HFE (4:6)) with almost conventional salt concentrations was designed, which is also the result we expected. Molecular dynamics (MD) results show that the micro-state of 1.2M-LiFSI-SL/HFE is more similar to that of 3M-LiFSI-SL, and very different from that of the 1M-LiFSI-SL, which is what we hope (Figure 1a). As the LiFSI salt concentrations increases, the number of Li^+ coordinated with SL molecules reduces from 3.5550 to 2.9373, while the FSI^- coordination number gradually increases from 2.4413 to 3.0032, suggesting more FSI^- enter the inner of solvation layer, forming novel solvation structures. In 1.2M-LiFSI-SL/HFE, the number of Li^+ coordinated with SL solvent molecules and the FSI^- are 2.9264 and 2.9998, respectively. These values are basically the same as before adding HFE solvent. The coordination number of HFE is 0.0006, indicating the addition of HFE did not coordinate with Li^+ and change the salt anions-dominated coordination situation of 3M-LiFSI-SL. Moreover, the poor wettability of 3M-LiFSI-SL can be addressed by the adding of HFE diluent. Compared to 3M-LiFSI-SL electrolyte which does not wet the separator, 1.2M-LiFSI-SL/HFE electrolyte can effectively spread on the separator (Figure S1, Supporting Information). Considering the reshaped anion-dominated solvation structure and reduced viscosity, we chose the designed 1.2M-LiFSI-SL/HFE electrolyte for further performance studies.

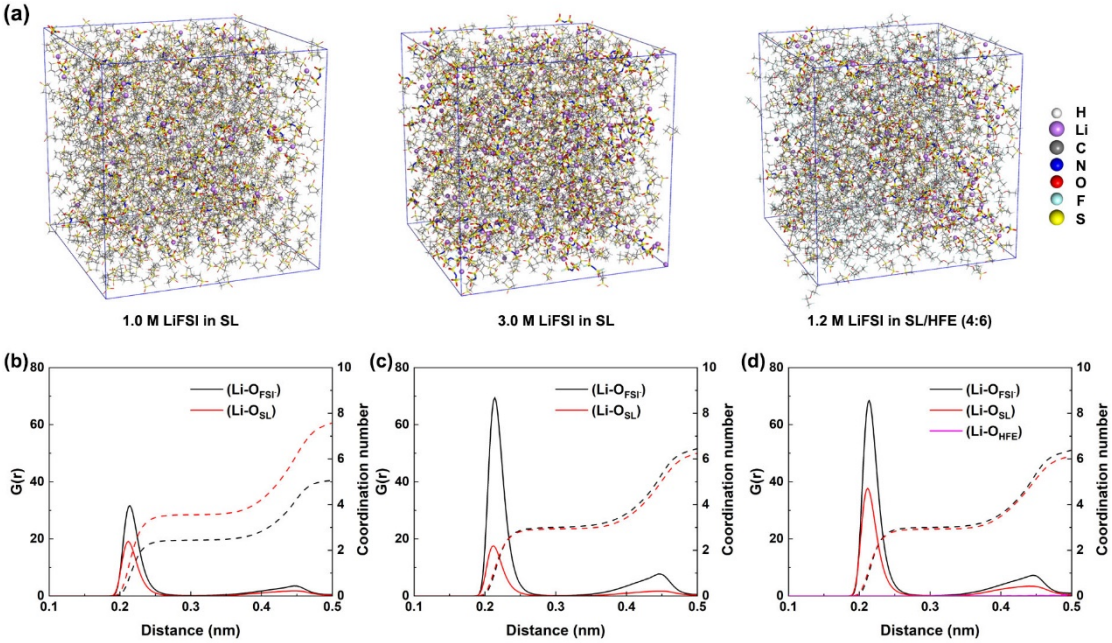

Figure 1. a) Molecular dynamics (MD) simulation results of 1M-LiFSI-SL, 3M-LiFSI-SL, and 1.2M-LiFSI-SL/HFE. b-d) Radial distribution function and coordination number of 1M-LiFSI-SL, 3M-LiFSI-SL, and 1.2M-LiFSI-SL/HFE, respectively.

The TR characteristics of practical pouch-type NCM811|Gr cells were investigated by accelerating rate calorimetry (ARC), which can effectively define three key temperatures $\{T_1, T_2, T_3\}$.[30] In detail, T_1 is the self-generated heat temperature of the practical cell, and T_2 ($dT/dt = 60\ ^oC\ min^{-1}$) is identified as the TR trigger temperature. After this, the cell soon reaches the maximum TR temperature T_3.[31,32] Increasing T_1, maximizing T_2, and minimizing T_3 are critical to improving safety of LIBs. The Ah-

level NCM811|Gr pouch cell employing conventional EC-containing electrolyte yields the self-generated heat T_1 of 137.9 °C, then the TR is triggered at 204.3 °C (T_2) (Figure 2a). Surprisingly, the T_1 and T_2 temperature of the NCM811|Gr cell with 1.2M-LiFSI-SL/HFE electrolyte can be enhanced up to 147.5 and 246.3 °C (Figure 2b), respectively. It is worth noting that the unique intermittent slow release of heat from 137.5 to 147.5 °C, indicating the decomposition of anion-induced inorganic-rich EEI of 1.2M-LiFSI-SL/HFE cell releases less heat than that of cell with conventional electrolyte. These results are further demonstrated by the thermal stability of the electrolyte and the charged anode (Figure S2, Supporting Information). Moreover, the TR highest temperature T_3 can be reduced to 639.7 °C. In summary, Ah-level NCM811|Gr pouch cell employing 1.2M-LiFSI-SL/HFE can efficiently improve self-generated heat T_1 by 9.6 °C, improve TR triggering temperature T_2 by 42.0 °C, and decrease the TR highest T_3 by 55.6 °C. Attributed to the robust and stable anion-induced EEI and weakened electrode/electrolyte exothermic reaction, the intrinsic safety of practical NCM811|Gr pouch cell employing 1.2M-LiFSI-SL/HFE can be greatly enhanced.

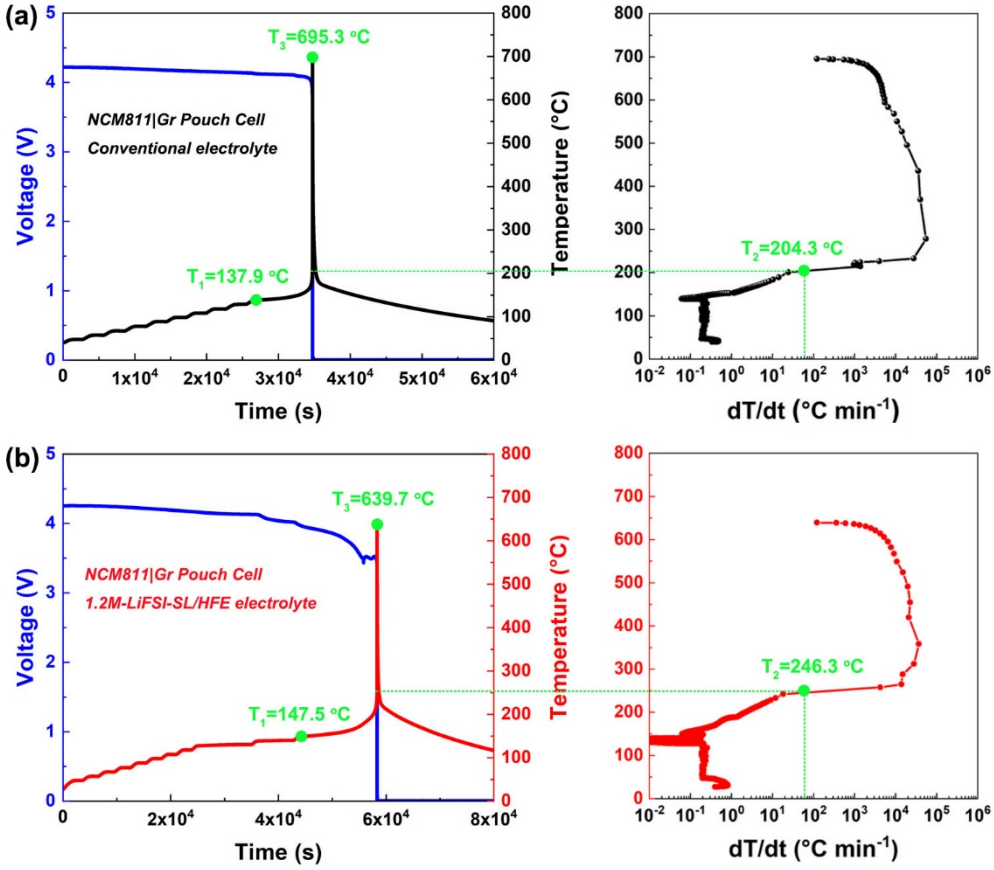

Figure 2. Thermal runaway characteristics of practical NCM811|Gr pouch cells. a) Cell employing conventional electrolyte b) Cell employing 1.2M-LiFSI-SL/HFE electrolyte.

The electrochemical characteristics of Ah-level NCM811|Gr pouch-type cells at 4.5 V and 1/3 C with different electrolytes were displayed in Figure 3. Firstly, 1 M $LiPF_6$ in EC/EMC was used as the conventional electrolyte. With the simple adoption of SL solvent and high concentration strategy, the NCM811|Gr pouch cell with 3M-LiFSI-SL

yields no discharge capacity (Figure S3, Supporting Information), which is attributed to very poor wettability due to high viscosity. Interestingly, only adding a certain amount of HFE nonsolvating solvent to build 1.2M-LiFSI-SL/HFE electrolyte, which yields high initial discharge capacity of 1038.3 mAh (vs 956.9 mAh for conventional electrolyte). Moreover, the pouch cell employing 1.2M-LiFSI-SL/HFE electrolyte presents outstanding high-voltage and long-term cyclability, that is, 88% capacity retention after 1000 cycles at 4.5V (Figure 3a). In comparison, the NCM811|Gr cell with conventional electrolyte undergoes only 400 cycles and then rapidly decays in a "diving" manner. In addition, the discharge capacity and coulombic efficiency of NCM811|Gr cell show dramatic fluctuations from 300 cycles, which reveal the severe parasitic reactions between the conventional electrolyte and electrode under the aggressive high voltage cycling conditions. Moreover, 1.2M-LiFSI-SL/HFE electrolyte presents steady voltage profiles (Figure 3b,c), which further confirms the above results. The outstanding high-voltage long-term cyclability and high coulombic efficiency (>99.9%) of pouch cell with 1.2M-LiFSI-SL/HFE electrolyte prove the formation of anions-derived robust EEI via reshaped Li^+ solvation structure, which can effectively prevent side reaction.

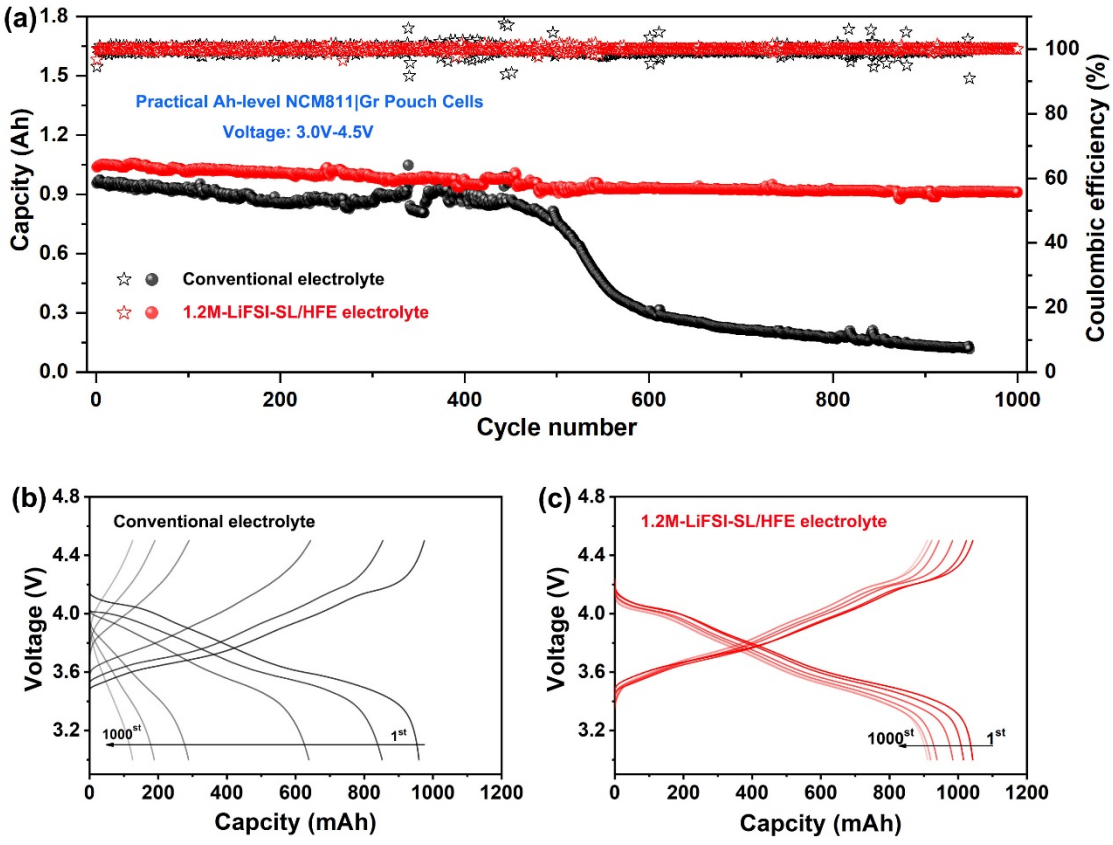

Figure 3. Electrochemical behavior of NCM811|Gr pouch cells. a) Cycling stability of NCM811|Gr employing conventional and 1.2M-LiFSI-SL/HFE electrolyte charged up to 4.5 V. b,c) Charge–discharge profiles of NCM811|Gr employing conventional and 1.2M-LiFSI-SL/HFE electrolyte charged up to 4.5 V, respectively.

The formation of EEI to stabilize electrode plays the vital roles on the safety and electrochemical characteristics of LIBs.[16,33] The chemistry and structure of the solid-electrolyte interphase (SEI) were characterized employing XPS and ToF-SIMS (Figure 4), respectively. The F 1s spectra of graphite anode reveal that SEI formed by the 1.2M-LiFSI-SL/HFE electrolyte contains more LiF species, evidenced by the higher intensity of LiF peak at 685 eV (Figure 4a,d).[13] Moreover, the N 1s and S 2p spectra are conducted to further confirm the chemical compositions. The N (Figure 4b,e) and S (Figure 4c,f) species are only observed on SEI of the graphite employing 1.2M-LiFSI-SL/HFE electrolyte, which can effectively inhibit side reactions.[34] To further evaluate the SEI formed in different electrolytes, secondary-ion fragments (e.g., LiF_2^-, SO_2^-, SO_3^-, NO^-, and NO_2^-) were detected by using ToF-SIMS. As shown in Figure 4g-j, the significant strong signals of SO_2^-, SO_3^-, NO^-, and NO_2^- species were detected on the interphase of graphite cycled in the 1.2M-LiFSI-SL/HFE electrolyte, indicating the SEI contains more robust inorganic species derived from salt anions. These results of secondary-ion fragments are consistent with the above XPS results. Moreover, the rich and homogeneous distribution of fragments (LiF_2^-, SO_2^-, SO_3^-, NO^- and NO_2^- species) are distinctly observed by 3D-rendering image (Figure 4k). The anions-induced stable inorganic-rich SEI is beneficial to suppress parasitic reactions and support reversible Li^+-intercalation behavior (Figure 3c). In addition, the more inorganic components of the SEI with higher thermal stability effectively reduce the self-exothermic heat of the pouch cell prior to T1 temperature, which was demonstrated by features of the unique intermittent slow release (Figure 2b).

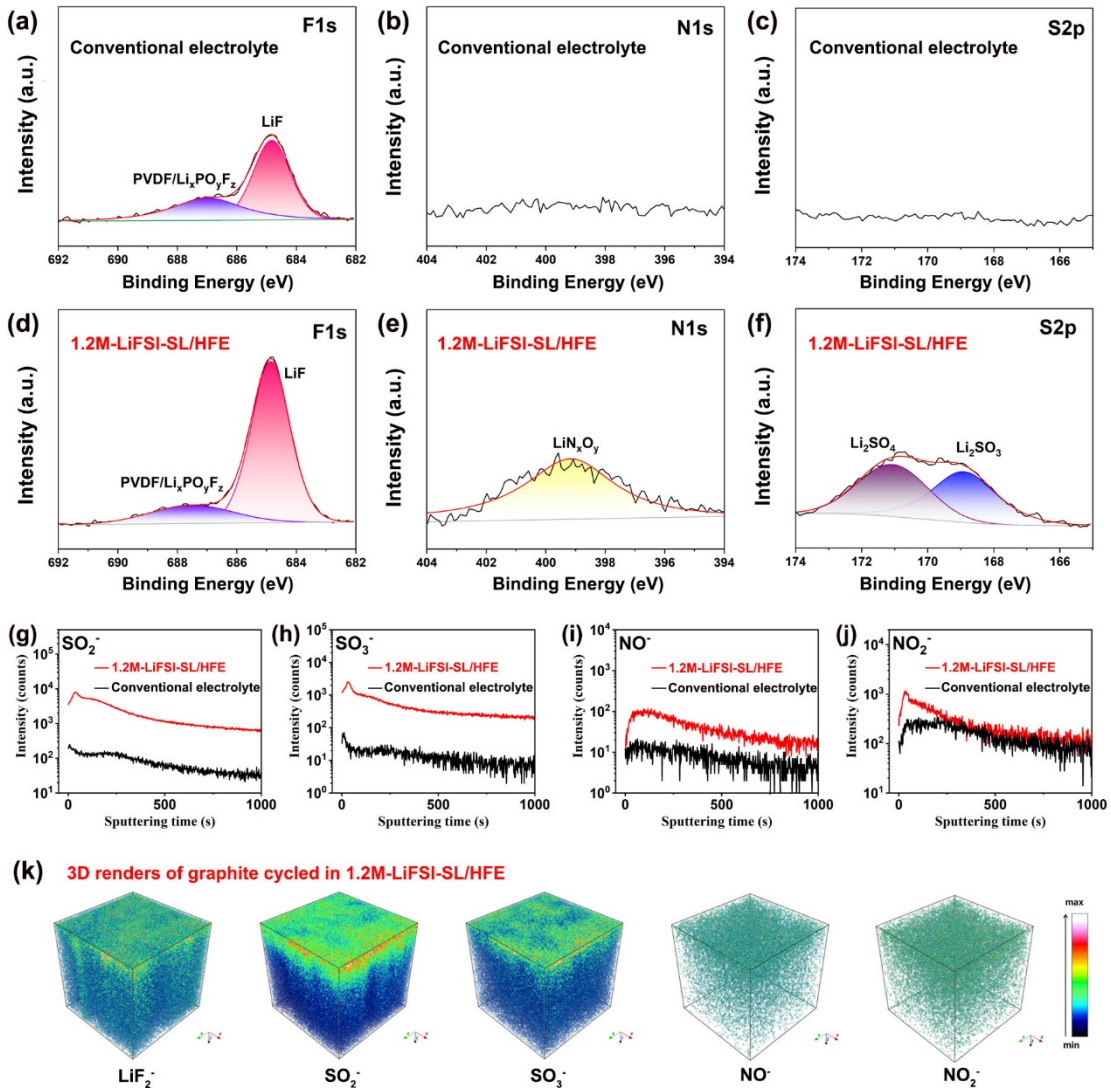

Figure 4. (a-f) XPS spectra of F1s, N1s, and S2p for the SEI of graphite cycled in conventional electrolyte a-c) and 1.2M-LiFSI-SL/HFE d-f). (g-j) ToF-SIMS spectra of the graphite cycled in different electrolyte. (k) 3D-rendering images of LiF_2^-, SO_2^-, SO_3^-, NO^- and NO_2^- species of the SEI of graphite cycled in 1.2M-LiFSI-SL/HFE electrolyte.

In addition to the anion-induced stable SEI formed on the graphite anode, the cathode electrolyte interphase (CEI) of the NCM811 is also a key factor.[13] The XPS was firstly used to investigate the chemical compositions of the surface of cycled NCM811 cathode. Similar to the chemistry of interphase formed on the cycled graphite anode, N (Figure S4a,c, Supporting Information) and S (Figure S4b,d, Supporting Information) signals are only found in CEI for the NCM811 employing 1.2M-LiFSI-SL/HFE electrolyte, which attributed to the decomposition of salt anions.[34] Plenty of fragments (e.g., LiF_2^-, CH_3O^-, SO_2^-, SO_3^-, NO^-, and NO_2^-) were obtained by using ToF-SIMS to reveal the depth distribution of the CEI formed on cycled NCM811 cathode (Figure 5). Compared to the uneven LiF_2^- species distribution of NCM811 cycled in conventional electrolyte (Figure S5a, Supporting Information), the interphase of NCM811 cycled in 1.2M-LiFSI-SL/HFE electrolyte presented the uniform X-Y and X-Z dimensional distribution

of inorganic LiF_2^- species (Figure S5b,c, Supporting Information). Moreover, the weaker organic CH_3O^- fragments signals were achieved (Figure S6, Supporting Information), indicating the interphase of NCM811 cycled in 1.2M-LiFSI-SL/HFE electrolyte contains less organic species.[33] The interphase of NCM811 cycled in 1.2M-LiFSI-SL/HFE electrolyte clearly presented a richer X-Y and X-Z dimensional distribution of fragments species (SO_2^-, SO_3^-, NO^-, and NO_2^-), attributed to the decomposition of salt anions (Figure 5e-h). Combining the high-voltage cyclability performances, the robust inorganic-rich CEI is beneficial to prevent from parasitic reactions.

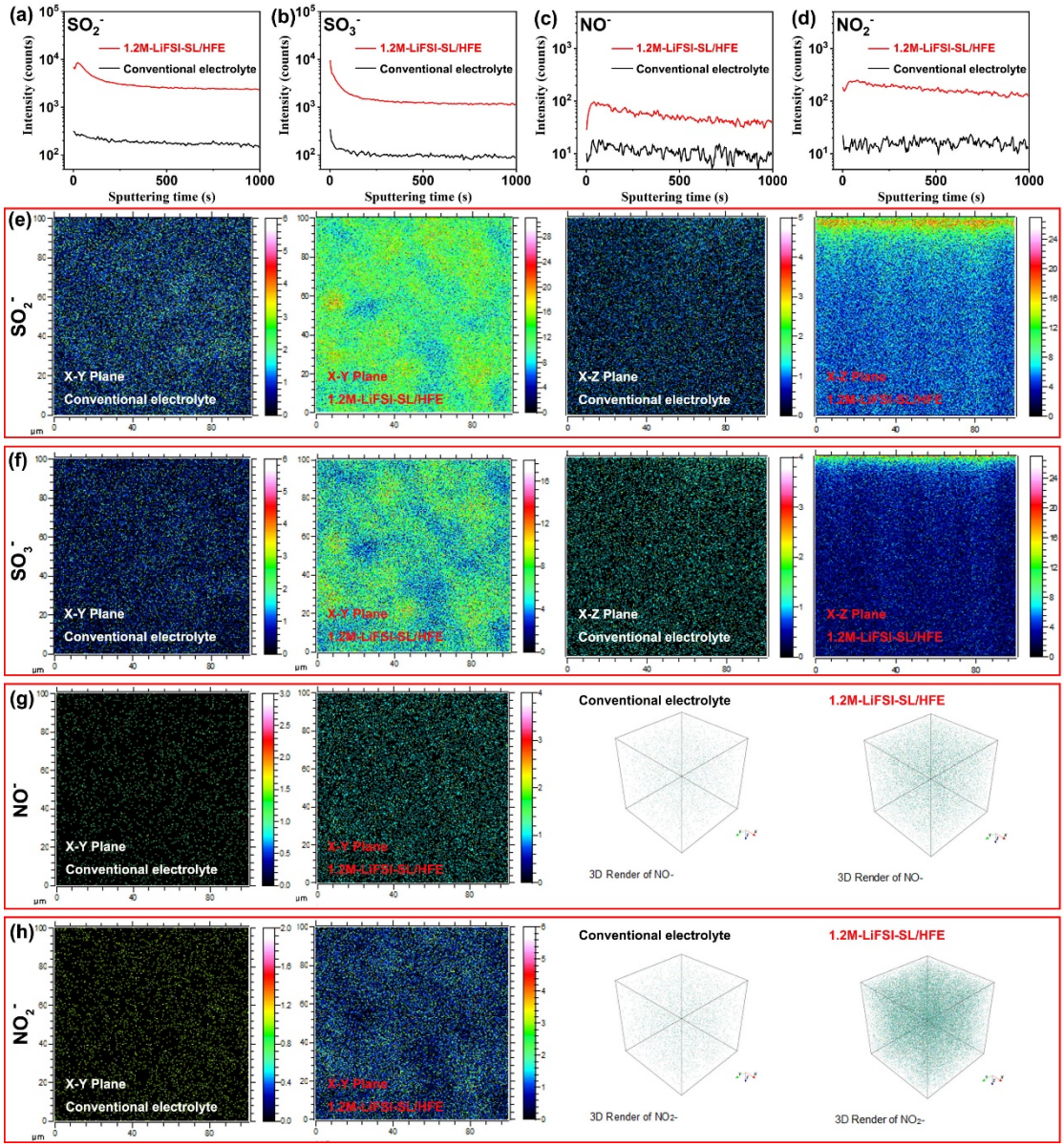

Figure 5. (a-d) ToF-SIMS spectra of the CEI formed on NCM811 cathode cycled in conventional electrolyte and 1.2M-LiFSI-SL/HFE electrolyte. (e-f) X-Y and X-Z plane chemical maps of SO_2^- and SO_3^- species of the CEI formed on NCM811 cathode. (g-h) X-Y plane and 3D-rendering images of NO^- and NO_2^- species of the CEI formed on NCM811 cathode.

CONCLUSIONS

By reshaping the anions-dominated Li^+ solvation structure, we developed SL-based electrolyte to build practical safer high-voltage and long cyclability pouch-type NCM811|Gr cells. Compared with the conventional electrolyte, NCM811|Gr cell with 1.2M-LiFSI-SL/HFE can effectively enhance self-generated heat T_1 by 9.6 ^oC, enhance TR triggering T_2 by 42.0 ^oC, and decrease the TR highest T_3 by 55.6 ^oC. More surprisingly, the pouch cell with 1.2M-LiFSI-SL/HFE exhibits outstanding capacity retention of 88% after 1000 cycles charged up to 4.5 V and increased initial discharge capacity of 1038.3 mAh (vs 956.9 mAh). The outstanding performances attributed to the substitution of the SL solvent for the EC solvent and construction of stable anions-derived inorganic-rich EEI, significantly protect electrode from side reactions. The work brings new insights for unlocking advanced electrolyte candidates to build next-generation practical safer high-energy LIBs.

EXPERIMENTAL PROCEDURES

Materials. Machine-made NCM811|Gr pouch-type cells were obtained dry (no electrolyte) from LiFun Technology (Xinma Industry Zone). The cells were transferred to an argon-filled glove box without exposure to ambient air, where they were filled with electrolyte, and the formation of the cells was performed at C/10 under 40 °C. The conventional electrolyte was purchased from Dodochem Ltd. LiFSI, 1,1,2,2-tetrafluoroethyl-2,2,3,3-tetrafluoropropyl ether (HFE), and SL were obtained from aladdin and dried over activated molecular sieves before use.

Safety tests. An EV-ARC manufactured by Thermal Hazard Technology was utilized for safety tests. A K type thermocouple was inserted into the center of cell to measure the internal temperature, which is used to evaluate the cell TR performance. During the TR tests, the EV-ARC was operated under the heat-wait-seek mode. A heating step of 5 ^oC with a wait time of 15 min was performed on the ARC starting from 40 ^oC. The EV-ARC system would go into the exotherm mode to track the temperature rise of tested batteries and maintain the adiabatic condition if the measured temperature rate exceeded 0.01 $^oC \cdot min^{-1}$.

Characterizations. Quantum chemistry calculations were first performed to optimize molecular geometries of SL and HFE solvent molecules using the Gaussian 16 package at B3LYP/6-311+G(d) level of theory. The atomic partial charges on these solvent molecules were computed by fitting to the molecular electrostatic potential at atomic centers with the Møller-Plesset second-order perturbation method and the correlation-consistent polarized valence cc-pVTZ(-f) basis set. The atomistic force field parameters for all ions and molecules are described by the AMBER format. The cross-interaction parameters between different atom types are obtained from the Lorentz-Berthelot combination rule. X-ray photoelectron spectroscopy (XPS) (PHI Quanteral II, Japan) was conducted to evaluate the chemical composition in the prepared electrodes. TOF-SIMS was applied to accurately reveal the chemical composition of the surface of NCM811 cathodes and Gr anodes via ToF.SIMS 5-100 instrument (IONTOF GmbH, Germany). A pulsed 30 keV Bi_3^{++} ion beam was set, and the selected analysis area was

100 × 100 um.

ACKNOWLEDGEMENTS

This study is supported by National Key R&D Program of China (Grant No. 2022YFB3807700), National Key Laboratory Foundation of Science and Technology on Materials under Shock and Impact (WDZC2022-2), National Natural Science Foundation of China (Grant No. 52004138 and 52076121), and Beijing Institute of Technology Research Fund Program for Young Scholars (XSQD-202210008). Research at the Argonne National Laboratory was funded by the U.S. Department of Energy (DOE), Vehicle Technologies Office. Support from Tien Duong of the U.S. DOE's Office of Vehicle Technologies Program is gratefully acknowledged. G.X. and K.A. acknowledge the support of the U.S. China Clean Energy Research Center (CERC-CVC2).

REFERENCES

[1] X. Y. Shan, F. Li, D. W. Wang, H. M. Cheng, *Energy Storage Mater.* **2016**, *3*, 66-68.
[2] D. Ren, X. Feng, L. Liu, H. Hsu, L. Lu, L. Wang, X. He, M. Ouyang, *Energy Storage Mater.* **2021**, *34*, 563-573.
[3] G.-L. Xu, Q. Liu, K.K.S. Lau, Y. Liu, X. Liu, H. Gao, X. Zhou, M. Zhuang, Y. Ren, J. Li, M. Shao, M. Ouyang, F. Pan, Z. Chen, K. Amine, G Chen, *Nat. Energy* **2019**, *4*, 484-494.
[4] X. Yang, D.D. Kieran, X. Gao, X. Sun, *eTransportation* **2022**, *11*, 100152.
[5] R. Li, W. Li, A. Singh, D. Ren, Z. Hou, M. Ouyang, *Energy Storage Mater.* **2022**, *52*, 395-429.
[6] K. Xu, *Chem. Rev.* **2004**, *104*, 4303-4418.
[7] K. Xu, *Chem. Rev.* **2014**, *114*, 11503-11618.
[8] N. Piao, X. Gao, H. Yang, Z. Guo, G. Hu, H. M. Cheng, F. Li, *eTransportation* **2022**, *11*, 100145.
[9] X. Fan, C. Wang, *Chem. Soc. Rev.* **2021**, *50*, 10486.
[10] H. Zhang, J. Zhang, *eTransportation* **2021**, *7*, 100105.
[11] W. Li, A. Dolocan, J. Li, Q. Xie, A. Manthiram, *Adv. Energy Mater.* **2019**, *9*, 1901152.
[12] S. Klein, S. V. Wickeren, S. Roser, et al, *Adv. Energy Mater.* **2021**, *11*, 2003738.
[13] Y. Wu, D. Ren, X. Liu, G. L. Xu, X. Feng, Y. Zheng, Y. Li, M. Yang, Y. Peng, X. Han, L. Wang, Z. Chen, Y. Ren, L. Lu, X. He, J. Chen, K. Amine, M. Ouyang, *Adv. Energy Mater.* **2021**, *11*, 2102299.
[14] Y. Li, X. Liu, L. Wang, X. Feng, D. Ren, Y. Wu, G. Xu, L. Lu, J. Hou, W. Zhang, Y. Wang, W. Xu, Y. Ren, Z. Wang, J. Huang, X. Meng, X. Han, H. Wang, X. He, Z. Chen, K. Amine, M. Ouyang, *Nano Energy* **2021**, *85*, 105878.
[15] Y. Wu, X. Feng, Z. Ma, L. Gao, Y. Wang, C.Z. Zhao, D. Ren, M. Yang, C. Xu, L. Wang, X. He, L. Lu, M. Ouyang, *eTransportation* **2023**, *15*, 100216.
[16] Y. Wu, X. Liu, L. Wang, X. Feng, D. Ren, Y. Li, X. Rui, Y. Wang, X. Han, G. L. Xu, H. Wang, L. Lu, X. He, K. Amine, M. Ouyang, *Energy Storage Mater.* **2021**, *37*, 77.

[17] Q. Li, X. Yu, H. Li, *eTransportation* **2022**, *14*, 100201.
[18] J. Alvarado, M. A. Schroeder, M. Zhang, O. Borodin, E. Gobrogge, M. Olguin, M.S. Ding, M. Gobet, S. Greenbaum, Y.S. Meng, K. Xu, *Mater. Today* **2018**, *21*, 341-353.
[19] Q. Zheng, G. Li, X. Zheng, L. Xing, K. Xu, W. Li, *Energy Environ. Mater.* **2022**, *5*, 906-911.
[20] S. Lin, H. Hua, P. Lai, J. Zhao, *Adv. Energy Mater.* **2021**, *11*, 2101775.
[21] X. Ren, S. Chen, H. Lee, D. Mei, M.H. Engelhard, S. D. Burton, W. Zhao, J. Zheng, Q. Li, M.S. Ding, M. Schroeder, J. Alvarado, K. Xu, Y.S. Meng, J. Liu, J.G. Zhang, W. Xu, *Chem* **2018**, *4*, 1877-1892.
[22] J. Fu, X. Ji, J. Chen, L. Chen, X. Fan, D. Mu, C. Wang, *Angew. Chem. Int. Ed.* **2020**, *59*, 22194-22201.
[23] K. Xu, W. Xu, S. S. Zhang, *J. Non-Cryst. Solids: X* **2022**, *14*, 100088.
[24] Y. Yamada, J. Wang, S. Ko, E. Watanabe, A. Yamada, *Nat. Energy.* **2019**, *4*, 269-280.
[25] X. Ren, L. Zou, S. Jiao, D. Mei, M.H. Engelhard, Q. Li, H. Lee, C. Niu, B.D. Adams, C. Wang, J. Liu, J.-.G. Zhang, W. Xu, *ACS Energy Lett.* **2019**, *4*, 896-902.
[26] S. Chen, J. Zheng, D. Mei, K.S. Han, M.H. Engelhard, W. Zhao, W. Xu, J. Liu, J.-G. Zhang, *Adv. Mater.* **2018**, *30*, 1706102.
[27] H. Jia, Z. Yang, Y. Xu, P. Gao, L. Zhong, D.J. Kautz, D. Wu, B. Fliegler, M.H. Engelhard, B. E. Matthews, B. Broekhuis, X. Cao, J. Fan, C. Wang, F. Lin, W. Xu, *Adv. Energy Mater.* **2023**, *13*, 2203144.
[28] S. Chen, J. Zheng, L. Yu, X. Ren, M.H. Engelhard, C. Niu, H. Lee, W. Xu, J. Xiao, J. Liu, J.-G. Zhang, *Joule* **2018**, *2*, 1548-1558.
[29] G. Song, Z. Yi, F. Su, L. Xie, Z. Wang, X. X. Wei, G. Xu, C. M. Chen, *ACS Energy Lett.* **2023**, *8*, 1336-1343.
[30] X. Feng, D. Ren, X. He, M. Ouyang, *Joule* **2020**, *4*, 743.
[31] X. Feng, M. Ouyang, X. Liu, L. Lu, Y. Xia, X. He, *Energy Storage Mater.* **2018**, *10*, 246-267.
[32] Y. Wang, X. Feng, W. Huang, X. He, L. Wang, M. Ouyang, *Adv. Energy Mater.* **2023**, *13*, 2203841.
[33] Y. Wu, X. Feng, X. Liu, X. Wang, D. Ren, L. Wang, M. Yang, Y. Wang, W. Zhang, Y. Li, Y. Zheng, L. Lu, X. Han, G. L. Xu, Y. Ren, Z. Chen, J. Chen, X. He, K. Amine, M. Ouyang, *Energy Storage Mater.* **2021**, *43*, 248-257.
[34] Y. Wu, X. Feng, M. Yang, C.-Z. Zhao, X. Liu, D. Ren, Z. Ma, L. Lu, L. Wang, G.-L. Xu, X. He, K. Amine, M. Ouyang, *Adv. Sci.* **2022**, *9*, 2204059.